

Phases of Underpotentially Deposited Hg on Au(111): An in Situ Surface X-ray Diffraction Study

Jun Li and Héctor D. Abruña*

Department of Chemistry, Baker Laboratory, Cornell University, Ithaca, New York 14853-1301

Received: November 19, 1996; In Final Form: February 3, 1997[⊗]

We report on an in situ surface X-ray diffraction study of the underpotential deposition (UPD) of mercury on Au(111). We have observed three UPD phases present at potentials prior to bulk mercury deposition. These phases consist of two well-ordered intermediate states and what appears to be either a fully discharged two-dimensional liquid Hg layer or a monolayer of an amorphous Hg–Au alloy. Both ordered intermediate phases have hexagonal structures with lattice vectors that are rotated 30° from those of the Au(111) substrate. The first phase (phase I), present at a potential of +0.68 V, was only observed on fresh flame-annealed Au(111) electrodes and appears to be an open incommensurate structure with a lattice constant of 3.86 ± 0.03 Å. This phase appears to be metastable since it changes to a second ordered phase (phase II) after a certain time at +0.68 V or after the potential is moved to more negative values (+0.63 V). The second phase has a more compact lattice with $a = 3.34 \pm 0.01$ Å and appears to be a commensurate 2×2 structure with $2/3$ of the Hg atoms at threefold hollow sites and $1/3$ on atop sites. Similar to the first one, this phase is also metastable and can be transformed to a final, fully discharged, state of a two-dimensional liquid Hg layer or an amorphous Hg–Au alloy. The entire Hg UPD process, from Hg^{2+} to the fully discharged metallic Hg layer, agrees well with a multistep mechanism based on previous electrochemical kinetic studies on polycrystalline Au electrodes. Our results also show that the UPD of Hg on Au(111) electrodes is quite different from that of other metals such as Cu, Ag, Tl, and Pb.

1. Introduction

The underpotential deposition (UPD) of monolayer or submonolayer amounts of metals onto foreign metal substrates is a fundamental electrochemical process which has attracted longstanding interest. The processes involved are also closely related to adsorption/desorption, charge transfer, nucleation and growth, and electrocatalysis. Within the UPD regime, the overlayer coverage and structure can be modulated and/or controlled by the electrode potential and the presence of coadsorbates, especially anions. The structures of UPD overlayers have been found to depend strongly on specific crystallographic planes and specific interactions. Much effort has been placed on correlating microscopic structures with electrochemical reactivities in UPD systems. In recent years, significant progress has been made in understanding UPD processes, in part due to the advent of in situ structural characterization techniques including scanning tunneling microscopy (STM),^{1,2} atomic force microscopy (AFM),³ and synchrotron X-ray scattering.^{4–6}

In this paper, we report on three distinct phases of Hg monolayers underpotentially deposited on Au(111) observed by in situ surface X-ray scattering measurements. This study follows our recent report on a coadsorbed structure of Hg_2^{2+} and SO_4^{2-} at the initial stages of Hg UPD.⁷ These studies present a very detailed picture of the microscopic processes involved in Hg UPD and agree well with previous electrochemical kinetic studies.

The Hg UPD process is of particular importance due to the special electrochemical properties of Hg surfaces and the formation of amalgams by Hg with a variety of metal substrates. There have been extensive studies of the electrodeposition of Hg on Au, especially polycrystalline surfaces, by conventional

electrochemical methods.^{8–12} It appears that mercury electrodeposition on polycrystalline gold electrodes involves some intermediate states and this was interpreted as being due to the presence of a mixture of Hg(0) and Hg(I) species (likely Hg_2^{2+}). These intermediate states are subsequently reduced to a full layer of metallic mercury. It has also been found that the mercury overlayer is stable in the UPD regime (i.e., at submonolayer coverage). Once the coverage exceeds one monolayer, the Hg atoms appear to diffuse into the bulk Au crystal to form an alloy (amalgam). However, this process is not well understood because of the lack of detailed microscopic structural information.

Salié and Bartels^{13–16} found that in perchloric acid solutions containing Hg(I) or Hg(II), the UPD of mercury involves a nonintegral partial charge transfer. Two different processes were detected during the deposition of Hg(I) at polycrystalline Au electrodes in the underpotential range by potentiostatic measurements at a rotating ring-disk electrode^{13–15} and by impedance spectroscopy.¹⁶ The first process was proposed to be the adsorption of metal ions onto the gold substrate surface to form an intermediate species with a partial charge of about $0.53e^-$ per Hg atom. The second process, whose kinetics appeared to be substantially slower, was one in which the partially charged Hg ions were completely discharged to form a full overlayer of metallic Hg. The first process can be thought of as chemisorption where the chemical bonds of adsorbed ions with the substrate metal lattice and surrounding electrolyte species determine the partial charge of the adsorbed ions. The second process would correspond to the completion of the full UPD layer and the onset of alloy formation. Within the UPD regime, measurements taken in Hg(II) solutions were found to be essentially the same as in Hg(I) solutions. Vicente-Beckett¹⁷ also found, by potentiostatic measurements at a rotating gold

[⊗] Abstract published in *Advance ACS Abstracts*, March 1, 1997.

ring-disk electrode, that the UPD of Hg in sulfuric acid solution is similar to that in perchloric acid media.

We report here direct in situ surface X-ray diffraction evidence of two intermediate phases of UPD Hg layers during the electrodeposition process and propose a mechanism for the entire process which is consistent with previous electrochemical studies.

There have been previous AFM and STM studies intended to derive the atomic structures of Hg UPD overlayers on Au(111). Using AFM, Gewirth and co-worker¹⁸ investigated the structure of UPD Hg overlayers in four different supporting electrolytes and revealed a strong dependence of the Hg overlayer structure on the nature of the anions. They found that, in sulfate, nitrate, and perchlorate electrolytes, the overlayer presented the same open hexagonal lattice with a lattice constant $a = 5.8 \pm 0.2 \text{ \AA}$ at potentials just prior to bulk deposition and a close-packed hexagonal lattice with an atom–atom spacing of $a = 2.9 \pm 0.3 \text{ \AA}$ just after bulk deposition. On the other hand, in acetate solutions, the Hg overlayer presented a close-packed hexagonal lattice with $a = 3.1 \pm 0.2 \text{ \AA}$ just prior to bulk deposition. At more positive potentials, they found two additional open structures.

However, in recent in situ STM studies, Itaya and co-workers¹⁹ found that the structure of the Hg adlayer at the first stage of UPD in sulfuric acid is different from that in perchloric acid. In both cases, the Hg overlayers present commensurate open rectangular lattices which are different from the hexagonal lattice reported by Gewirth.¹⁸ Although there is a clear discrepancy in these results, they both indicate a strong effect of supporting electrolyte anions on the resulting Hg UPD structures. It is also clear that mercury appears to form ordered adlayers when the deposition is within the monolayer regime. The ambiguity in the specific Hg adlayer structure may actually be due to anions adsorbed on top of the Hg adlayer since both AFM and STM are most sensitive to the topmost surface. The strong tip–adsorbate interaction makes it difficult for STM and AFM techniques to probe the real undisturbed overlayer structure.

On the other hand, synchrotron radiation based surface X-ray diffraction has the advantage over STM and AFM techniques in that X-ray photons penetrate down to the bulk substrate without any disturbance to the overlayers. Thus X-ray scattering measurements can probe the precise undisturbed multilayer structure along the surface normal as well as the atomic arrangement within each layer. This is extremely valuable particularly for UPD processes which often involve the coadsorption of other electrolyte species.

In a recent paper,⁷ we reported that there appears to be a highly ordered coadsorbed structure in the first stage of Hg UPD on Au(111) (at $+0.80 \text{ V} \leq E \leq +0.88 \text{ V}$ vs Ag/AgCl(3 M KCl)). This structure consists of a distorted honeycomb lattice of mercurous (Hg_2^{2+}) ions (0.375 monolayer of Hg_2^{2+}) with sulfate anions adsorbed in the hollow sites (0.375 monolayer) and above the plane of Hg(I). This study agreed well with electrochemical data²⁰ and explained the very sharp peaks in the cyclic voltammogram at $+0.93 \text{ V}$. We believe that the large open lattices observed by STM and AFM likely arise from the disturbed sulfate anions instead of Hg adlayers, as has been previously found for Cu UPD on Au(111).^{1–3}

However, there is still a lack of detailed information about the additional stages of Hg UPD on Au(111) in sulfuric acid solutions where a full monolayer of metallic Hg is formed just prior to bulk deposition. STM images are very difficult to acquire at these potentials due to the electrochemical oxidation of mercury that takes place at the tip electrode.¹⁹ AFM studies

by Gewirth et al.¹⁸ found a close-packed hexagonal overlayer (with $a = 2.9$ to $3.1 \pm 0.3 \text{ \AA}$) in all four electrolytes. This suggests that an ordered metallic Hg monolayer is indeed formed on Au(111) surfaces in all cases.

In this paper, we report on three additional phases present during Hg UPD on Au(111) in sulfuric acid solutions. Two of these phases are ordered Hg adlayer structures which are present as intermediate states. The third and final state of Hg UPD just prior to bulk deposition represents a monolayer of two-dimensional liquid Hg or an amorphous Hg–Au alloy. These three phases were revealed by synchrotron-based surface X-ray scattering studies. The paper is organized as follows. The experimental details (section 2) will be briefly discussed first and then the electrochemical behavior of Hg UPD on Au(111) electrodes is presented in section 3.1. The grazing incidence X-ray diffraction (GIXD) measurements of the two ordered Hg UPD phases and corresponding in-plane real space structures will be presented next (section 3.2). Specular crystal truncation rod (CTR) measurements of both phases are presented in section 3.3 to reveal the structure along the surface normal. In section 4, we discuss the time dependence of these two Hg UPD phases and correlate the structures with the deposition mechanism. Conclusions are presented in section 5.

2. Experimental Section

The experimental setup and measurement conditions were described in detail in our previous report.⁷ A Au(111) single-crystal disk ($\sim 9 \text{ mm}$ in diameter and $\sim 2 \text{ mm}$ thick) was used as the working electrode for both electrochemical and X-ray scattering measurements. The crystal was chemically etched and flame-annealed before being placed in the X-ray scattering cell. A Ag/AgCl (3 M KCl) reference electrode was used without regard for the liquid junction. A coil of platinum wire was employed as the counter electrode. High-purity H_2SO_4 (J. T. Baker) and ultrapure water (Milli-Q) were used to prepare solutions. Solutions containing Hg^{2+} were prepared by dissolving HgO (Alfa, 99.998%) into appropriate solutions. Electrochemical experiments were carried out with a BAS CV-27 potentiostat and recorded with a BAS X-Y recorder. In some cases, a PAR 283 potentiostat interfaced with Corrware software was employed.

X-ray diffraction experiments were performed at the Exxon X10B beamline at the National Synchrotron Light Source using a four-circle diffractometer. X-ray photons of 1.1287 \AA wavelength were employed. The sample cell has a reflection geometry with the crystal at the center. X-ray photons penetrate through a 2.5 \mu m Mylar film (Chempix) as well as a thin film of electrolyte (estimated to be $\sim 30 \text{ \mu m}$ thick) covering the Au(111) crystal. During X-ray scattering measurements, the electrolyte was withdrawn to achieve a thin layer configuration in which the background and absorption were reduced. Each time the potential was changed to a new value, the Mylar film was inflated by adding more electrolyte and held in this condition for about 5 min to ensure equilibration. Typically, a complete specular CTR measurement takes about 6–8 h. However, the freshly deposited intermediate Hg phases were found to be stable only for 3–6 h. To ensure that we were measuring the same structure, we stripped and redeposited Hg adlayers every 2 h.

In this paper, the X-ray reflections are referred to the reciprocal lattice units of the hexagonal coordinates of the Au(111) substrate, with \mathbf{a}_s and \mathbf{b}_s along the nearest-neighbor direction in the surface plane ($a_s = b_s = 2.885 \text{ \AA}$) and \mathbf{c}_s ($c_s = 2.356 \text{ \AA}$) normal to the Au(111) plane. The \mathbf{Q} vectors are described by two components with $Q_{\parallel} = h\mathbf{a}_s^* + k\mathbf{b}_s^*$ in the

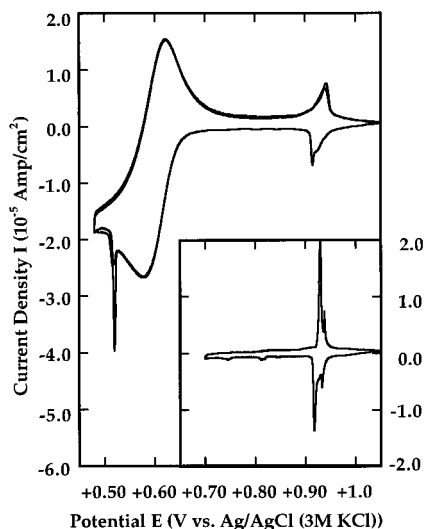


Figure 1. Cyclic voltammogram of a Au(111) electrode in 0.10 M sulfuric acid containing 1.0 mM Hg^{2+} at a scan rate of 2 mV/s. Inset: voltammogram profile over the range of +1.05 to +0.70 V vs Ag/AgCl (3 M KCl).

surface plane and Q_z along the surface normal. GIXD measurements were carried out in azimuth fixed mode where the incident and outgoing angles were kept small ($\alpha = \beta \approx 3.5^\circ$, at $L = 0.1$ reciprocal lattice unit (rlu)) so as to reduce the background and absorption by the Mylar film and electrolyte solution. A complete CTR measurement consists of a series of rocking curves at Q_z 's from 0 to 2 rlu. Each of these rocking curves was fitted to a Lorentzian line shape to derive the integrated intensity which was subsequently used for fitting.

3. Results

3.1. Cyclic Voltammetry. Figure 1 shows the cyclic voltammogram of a Au(111) electrode in 0.10 M H_2SO_4 containing 1.0 mM Hg^{2+} at a scan rate of 2 mV/s, which is similar to that reported by Itaya and co-workers.¹⁹ The inset shows the voltammogram when the potential is cycled between +0.70 and +1.05 V, where one can observe two sets of very sharp peaks around +0.93 V. In addition, there are two much smaller and broader peaks at +0.74 and +0.81 V, respectively. As discussed in our previous paper,⁷ the two sets of sharp peaks around +0.93 V correspond to the desorption of preadsorbed sulfate anions and the deposition of Hg_2SO_4 . An ordered coadsorbed structure of Hg_2SO_4 was observed at potentials $+0.80 \leq E \leq +0.88$ V. The sharpness of these features would suggest that these processes are quite rapid. The nature of the small waves at +0.81 and +0.74 V is not clear at this time. Upon further scanning the potential to more negative values, a broad and diffusional-like reduction peak appears at +0.60 V, as shown in the main panel of Figure 1. There is also a very sharp spike at +0.52 V superimposed on the broad reduction wave. However, no corresponding oxidation peak is observed if the scan direction is reversed after it passes this spike. Instead, only a broad oxidation peak, corresponding to the broad reduction peak, appears. Once the electrode potential is scanned beyond the sharp spike at +0.52 V, both the sharp double peaks at +0.93 V and the single peak at +0.52 V are dramatically broadened and diminished in amplitude in successive scans. This change is clearly evident when comparing the main panel with the inset to Figure 1. However, if the scan direction is reversed right on the sharp spike at +0.52 V, a sharp oxidation spike also appears on the anodic sweep and the change in the double peaks at +0.93 V is greatly minimized. The broad peak at

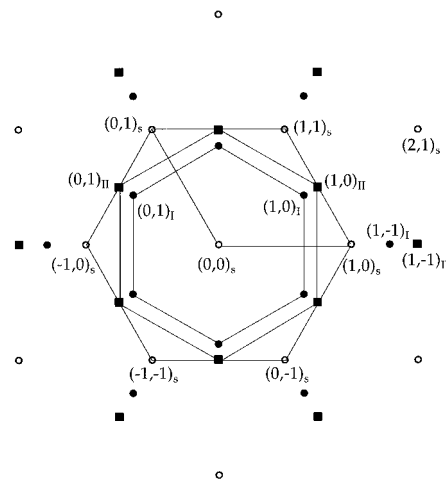


Figure 2. Reciprocal space map of the in-plane diffraction from Hg UPD phase I (solid circles) and Hg UPD phase II (solid squares) relative to that of Au(111) surface (open circles). The reflections from Au(111) surface are indexed as $(h,k)_s$ and those from Hg UPD phase I and phase II are indexed as $(h,k)_I$ and $(h,k)_II$, respectively.

+0.60 V appears to correspond to the deposition of the first Hg monolayer and the sharp spike at +0.52 V likely indicates the completion of the Hg monolayer and the onset of amalgam formation. The sharp feature at +0.93 V is consistent with our previously reported coadsorption structure which is reversible and has rapid kinetics. On the other hand, the broad diffusional-like feature between +0.50 and +0.70 V suggests a slow process. This might be accounted by the existence of intermediate states during the reduction of Hg(I) to Hg(0) , as indicated in previous electrochemical studies on polycrystalline Au.^{13–17} In this paper, we will focus on the structure and kinetics of Hg UPD layers at potentials within this broad wave.

3.2. Grazing Incidence X-ray Diffraction Results. GIXD measurements were taken at a series of potentials from +1.05 to +0.50 V at 50 mV intervals. As we described in our previous paper, an ordered coadsorbed structure of Hg_2SO_4 was found at $+0.80 \text{ V} \leq E \leq +0.88 \text{ V}$. When the potential was changed to approximately +0.68 V (the onset of the broad reduction wave), we found an ordered hexagonal structure corresponding to a Hg UPD adlayer (referred to as UPD phase I). This structure was transformed to the second ordered hexagonal structure (referred to as UPD phase II) when the potential was moved to values below +0.63 V but above that of bulk deposition (around +0.45 V).

Figure 2 shows the experimentally observed in-plane diffraction spots of Hg UPD phase I and phase II relative to the Au(111) substrate. The open circles represent the reciprocal lattice points of the Au(111) surface which are indexed as $(h,k)_s$. The solid circles are the measured diffraction spots from the Hg UPD phase I (indexed as $(h,k)_I$) and the solid squares are from the Hg UPD phase II (indexed as $(h,k)_II$). Both of these Hg UPD phases have hexagonal lattices rotated by 30° relative to the Au(111) substrate orientation. The diffraction spots from Hg UPD phase II fall on, within our experimental error ($<0.5\%$), the spots indexed with the substrate coordinates $(h/2, k/2)_s$ (with h, k as integers), indicating that the overlayer is likely commensurate with the Au(111) substrate. On the other hand, Hg UPD phase I is clearly incommensurate with the substrate surface. For both structures, higher order reflections at $(1,-1)_I$, $(2,1)_I$, and $(1,-1)_{II}$, $(2,1)_{II}$ were also observed, which unambiguously defined the hexagonal lattice of the Hg UPD adlayers.

From the size and geometry of the reciprocal lattice, we can derive the hexagonal real space lattice of the Hg adlayers as

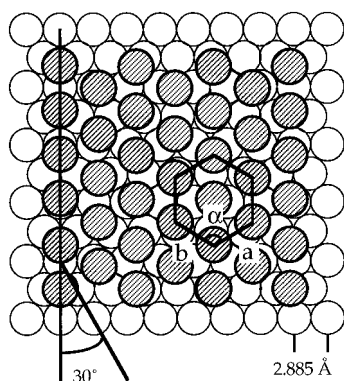


Figure 3. Schematic of the real space model of Hg UPD phase I.

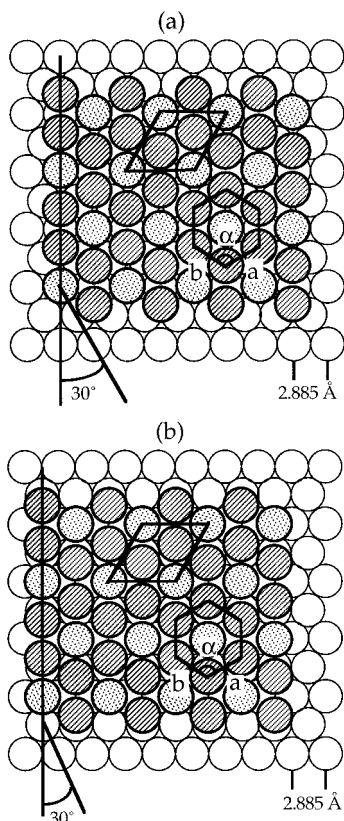


Figure 4. Schematics of two possible commensurate real space structural models of Hg UPD phase II.

shown in Figures 3 and 4, respectively. Figure 3 shows the incommensurate structure of Hg UPD phase I with lattice constants $a = b = 3.86 \pm 0.03 \text{ \AA}$ and $\alpha = 60^\circ$. The error bar is calculated from the standard deviation of measurements at different spots and with different samples. The open circles represent substrate atoms of the Au(111) surface, and the hatched circles are the Hg atoms (with a diameter of 3.01 \AA). If the first Hg atom is placed in a threefold hollow site, the other Hg atoms clearly do not fall on any specific sites, indicating that the overlayer is incommensurate with the substrate. The lattice constant of this structure is 28.2% larger than the nearest neighbor distance in bulk Hg (3.01 \AA). Considering that this structure might correspond to one of the partially charged states,^{13–17} the expanded lattice can be readily rationalized by the Coulombic repulsion between partially charged Hg atoms.

Hg UPD phase II also has a hexagonal lattice with lattice parameters $a = b = 3.34 \pm 0.01 \text{ \AA}$ and $\alpha = 60^\circ$. The lattice constant of this structure is still 11% larger than the nearest Hg–Hg distance in frozen bulk Hg. However, this lattice can

be superimposed on a commensurate $c(2 \times 2)$ structure, as shown in Figure 4. In Figure 4a, one-third of the Hg atoms (dots filled circles) sit on atop sites while the other two-thirds of the Hg atoms (hatched circles) sit at threefold hollow sites. The nearest Hg–Hg distance in this structure is 3.3313 \AA which is within the error of our experimental results. The lattice expansion in this case is probably due to the Hg–substrate interactions for forming a commensurate structure rather than to Coulombic repulsion as in Hg UPD phase I. We can correlate this structure with an intermediate state with nearly zero charge as has been previously proposed based on electrochemical studies.^{13–17} However, experimentally, we did not observe any diffraction corresponding to the 2×2 superlattice. This might be because the small surface corrugation of the Au(111) gives rise to little modulation to the heights of overlayer atoms to which grazing incidence X-ray diffraction is not very sensitive. This has also been the case for other UPD systems on Au(111) and Ag(111) electrodes.^{21,22}

With the in-plane diffraction data alone, we cannot unambiguously establish the exact registry of the Hg atoms on the Au(111) surface. Figure 4b shows an alternate model which is also consistent with the in-plane diffraction data. This one is also a $c(2 \times 2)$ commensurate structure with one-third of the Hg atoms (dots filled circles) located at bridge sites and the other two-thirds of the Hg atoms (hatched circles) located at quasi threefold hollow sites. In principle, the two models shown in Figure 4 could be distinguished by fitting the intensity profile along L at nonspecular spots, i.e., nonspecular rod scans. However, a detailed structural determination by this method requires a large amount of data taken with a highly ordered and stable system and has only been successfully demonstrated in the model system of Cu UPD on Au(111).²³ In the present case of Hg UPD, the metastable nature of the Hg UPD layers prevented us from carrying out a reliable measurement of nonspecular rods.

The in-plane radial scans across the first-order diffraction spots $(1,0)_s$ from the Au(111) surface, $(1,0)_I$ from Hg UPD phase I, and $(1,0)_{II}$ from Hg UPD phase II are shown in Figure 5, a, b, and c, respectively. The diffraction from the Au(111) surface is better fitted with a Lorentzian rather than a Gaussian distribution. The fitted full width at half-maximum is $0.00549 \pm 0.00036 \text{ \AA}^{-1}$ which is limited by the detector slit. However, it establishes that the coherence length of the Au(111) surface is at least $1144 \pm 40 \text{ \AA}$.

In-plane radial scans of both Hg UPD phases are better fitted with Gaussians than Lorentzians. The scan of Hg UPD phase I in Figure 5b is slightly asymmetric due to the tail from a nearby mosaic (within 0.1° in azimuth) picked up by the relaxed detector resolution. Therefore, it was fitted with an additional Gaussian to account for the small tail. The major peak was fitted with a width of $0.0165 \pm 0.0016 \text{ \AA}^{-1}$ which corresponds to a coherence length of about $380 \pm 37 \text{ \AA}$. The scan of Hg UPD phase II in Figure 5c can be fitted with one Gaussian. The width is $0.0139 \pm 0.00036 \text{ \AA}^{-1}$, smaller than that of Hg UPD Phase I. This gives rise to a larger coherence length of about $450 \pm 12 \text{ \AA}$.

Both Hg UPD phases have coherence lengths much smaller than the Au(111) substrate, indicating that they are not limited by the substrate quality. It is likely that the Hg adlayers form two-dimensional islands on the substrate surface rather than being homogeneously distributed. Since liquid Hg has a very large surface tension, it would not be surprising to observe the formation of 2-D islands. On the other hand, azimuthal scans (not shown) of both Hg UPD phases can be fitted with Lorentzians with a fwhm of $0.10^\circ \pm 0.015^\circ$, which is identical

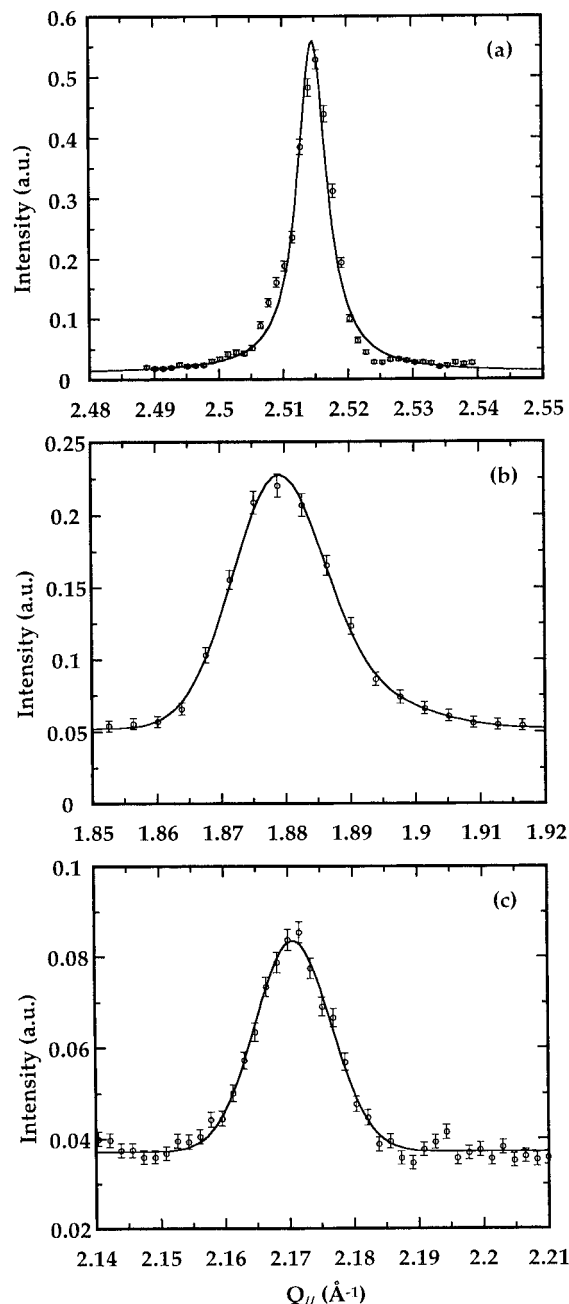


Figure 5. In-plane radial scans of (a) Au(111) substrate, (b) Hg UPD phase I, and (c) Hg UPD phase II. The Au(111) surface peak is fitted by a Lorentzian while the Hg UPD peaks are fitted with Gaussians.

to the Au(111) substrate. Therefore, no additional orientational disordering is introduced into the Hg adlayers.

The UPD of Hg on Au(111) is quite different from that of the neighboring metal elements in the same row of the periodical table, such as Tl, Pb, and Bi.^{21,22} The nearest-neighbor distances in bulk solids of Tl, Pb, and Bi are 3.46, 3.50, and 3.07 Å, respectively. All of these values are much larger than the 2.885 Å nearest Au–Au distance in bulk gold. The UPD layers of Tl and Pb just prior to bulk deposition on Au(111) and Ag(111) have been found to have essentially identical structures to their vapor-deposited counterparts in vacuum environments. In both cases, the UPD layers present incommensurate hexagonal lattices rotated by 2°–5° relative to the substrate orientation. The lattice parameters were found to be compressed by only about 3% from the bulk values and to decrease with decreasing electrode potential. On the other hand, the UPD layers of Bi on Au(111),²⁴ Tl on Au(100),²⁵ and Ag(100)²⁶ were found to

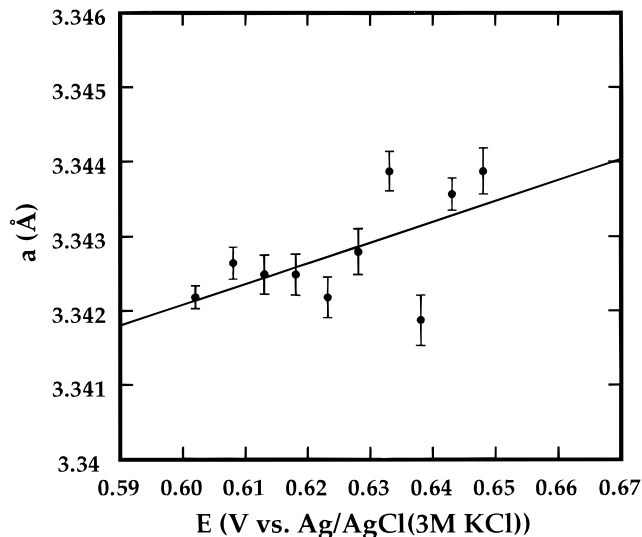


Figure 6. Potential dependence of the lattice parameter of Hg UPD phase II.

present uniaxially commensurate rectangular structures which were distorted from the bulk hexagonal structure. The incommensurate lattice was also compressed with decreasing electrode potential. Therefore, it appears that the adatom–adatom interactions in these systems are likely the most important while the adatom/substrate, the anion/substrate, and the anion/adatom interactions have little effect on the structure of the complete UPD monolayers.²¹

In contrast, the two ordered Hg UPD phases that we observed have expanded structures compared to frozen bulk Hg. Phase I was only observed in a rather narrow potential range (<50 mV). Within this range, we did not observe any clear potential dependence of the lattice parameters. However, the statistical error calculated from several samples deposited under different conditions is rather large. This is likely due to the metastable nature of this structure, which prevented us from carrying out a careful potential dependence study of this structure. On the other hand, Hg UPD phase II is more stable and has much smaller statistical errors. Figure 6 presents the potential dependence of the lattice parameter of Hg UPD phase II. In general, there is only a very small change, barely larger than the error bars. If fitted with a linear function, the slope of the line is about 0.028 Å/V, which is at least 1 order of magnitude smaller than the corresponding values of Tl, Pb, and Bi UPD on Au(111) and Au(100) surfaces.^{21,22,24–26} This provides an additional and strong evidence that Hg UPD phase II is a commensurate phase as we proposed above.

3.3. Specular CTR Results. It is important in our studies to relate the in-plane surface structure to the surface normal structure. This can be done with the complementary information derived from X-ray reflectivity studies, i.e., the measurement of the intensity profiles of specular crystal truncation rods. In these studies, the weak scattering between (0,0,L) Bragg reflections is very sensitive to the average density and arrangement of adsorbate layers.

In the case of in situ electrochemical studies, the specular CTR curve of a Au(111) crystal covered with an overlayer can be calculated as²⁷

$$R(0,0,L) = |T(Q_z)|^4 \left[\frac{256\pi^2 r_0^2}{3a_s^4 Q_z^2} \right] |s(0,0,L)|^2 e^{-Q_{\text{abs}}/Q_z} \quad (1)$$

where the sum over atomic layers is

$$s(0,0,L) = F_{\text{Au}}(Q_z) \sum_{n=1}^{\infty} \langle \rho_n e^{-Q_z^2 \sigma_n^2 / 2} e^{iQ_z n d} \rangle + \\ F_{\text{Au}}(Q_z) \langle \rho_0 e^{-Q_z^2 \sigma_0^2 / 2} e^{iQ_z(d_0 - d)} \rangle + \\ F_{\text{ads}}(Q_z) \langle \rho_{\text{ads}} e^{-Q_z^2 \sigma_{\text{ads}}^2 / 2} e^{iQ_z(d_{\text{ads}} - d_0 + d)} \rangle \quad (2)$$

In eq 1, $T(Q_z)$ is a factor that accounts for the enhancement at the critical angle and $\exp(-Q_{\text{abs}}/Q_z)$ accounts for the absorption by the polymer and electrolyte film with a constant thickness. The first term in eq 2 corresponds to the sum of the scattering amplitude over the bulk Au(111) layers. Each atomic layer is described by three parameters: the coverage or density ρ_m (defined as the atomic ratio of the species in the n th layer to that of Au atoms in a bulk Au(111) layer), the atomic root mean square (rms) displacement σ_m , and the interlayer distance d . We fixed these values at $\rho_m = 1$, $\sigma_m = 0.085 \text{ \AA}$, and $d = 2.3556 \text{ \AA}$ as reported for bulk Au(111) layers.²⁸ The second term corresponds to the scattering from the top Au(111) layer and the third term corresponds to that from the Hg UPD layer. The atomic scattering factors F_{Au} and F_{ads} were numerically calculated from the empirical equations in the International Tables for Crystallography.²⁹ The coverage of the top Au(111) layer was fixed at $\rho_0 = 1$ and the other parameters σ_0 , d_0 , ρ_{ads} , σ_{ads} , and d_{ads} were left free to vary during fitting.

Figure 7 shows the CTR data of the Au(111) electrode in 0.10 M H₂SO₄ containing 0.10 mM Hg²⁺ at (a) $E = +1.00 \text{ V}$ (solid circles), (b) $+0.68 \text{ V}$ (open squares), and (c) $+0.63 \text{ V}$ (open circles), respectively. The CTR data at $+0.68$ and $+0.63 \text{ V}$ correspond to Hg UPD phase I and II, respectively. Since one complete set of CTR measurements can take more than 8 h, during which time the Hg UPD structure might be changed, in-plane surface diffraction measurements were carried out periodically to ensure that the Hg UPD structure was the same. Data set at $+0.68$ and $+0.63 \text{ V}$ were shifted down by 1 and 2 orders of magnitude, respectively, in order to give a clearer view. The dashed lines are the CTR curves for an ideally truncated Au(111) surface and the continuous lines are the fits to the experimental data. The spikes at $L = 1$ and 2 correspond to the first- and second-order diffraction from the bulk Au(111) planes, respectively. Around the valleys ($L = 0.5$ and 1.5), the scattering from the substrate layers cancels out and thus the specular CTR intensity is most sensitive to the surface structure. Specifically, it provides the average electron density profile in a direction normal to the surface. It is clear that, in all cases, the data show deeper valleys than the ideal Au(111) surface. This cannot be accounted for with just an enhanced rms displacement of Au(111) surface atoms. Instead, adsorbed overlayers have to be incorporated onto the surface in order to fit the data. The scattering from adsorbates interferes with that from the Au(111) substrate and thus gives rise to deeper valleys in the CTR profiles.

The fitted parameters at the three potentials are listed in Table 1. At $E = +1.00 \text{ V}$, the CTR data are identical to those measured in pure 0.10 M H₂SO₄ solution at the same potential. The data can be fitted with a sulfate/bisulfate overlayer of density $\rho_{\text{ads}} = 0.371 \pm 0.02$, as shown in Figure 7a. As discussed in our previous paper, this density is in agreement with both a 0.40 monolayer of bisulfate and a 0.20 monolayer of sulfate incorporating some water or hydronium ions (≥ 0.4 monolayer). The fitting was relatively insensitive to the overlayer rms displacement σ_{ads} . Thus, it was fixed at 0.20 \AA during fitting. The distance between the overlayer and the first substrate layer, d_{ads} , was found to be $2.082 \pm 0.038 \text{ \AA}$ which is also in agreement with the value obtained in pure 0.10 M H₂SO₄ solution. The rms displacement of the Au(111) surface was

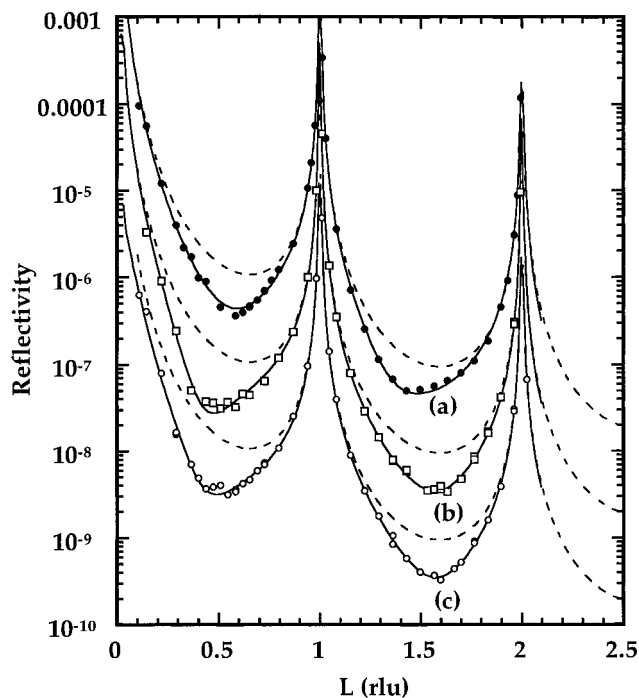


Figure 7. CTR of the Au(111) electrode in 0.10 M H₂SO₄ containing 0.10 mM Hg²⁺ measured at $E = +1.00 \text{ V}$ (a, solid circles), $+0.68 \text{ V}$ (b, open squares), and $+0.63 \text{ V}$ (c, open circles). The data at $+0.68$ and $+0.63 \text{ V}$ correspond to Hg UPD phases I and II, respectively. Each set of data is shifted down by 1 order of magnitude relative to the previous one to give a better view. The dashed lines are the calculated CTR curves for an ideally truncated Au(111) crystal. The continuous lines are the fits to the experimental data with a multilayer model.

enhanced from 0.085 \AA (bulk value) to $0.184 \pm 0.012 \text{ \AA}$ due to the strong chemical interaction of the adsorbed sulfate/bisulfate anions. The top layer to second layer distance was only slightly expanded from 2.356 \AA to $2.406 \pm 0.004 \text{ \AA}$.

As mentioned earlier, at $E = +0.68 \text{ V}$, we observed the in-plane diffraction of Hg UPD phase I. The CTR curve (Figure 7b) at this potential is quite different from curve 7a with a deeper valley around $(0, 0, 1/2)$ which is asymmetrically shifted to a lower value of L . In contrast to the two-layer coadsorbed structure at $+0.80 \text{ V} \leq E \leq +0.88 \text{ V}$ in our previous paper,⁷ this set of CTR data can be fitted with a single Hg overlayer on the relaxed Au(111) surface. The Au(111) surface rms displacement and the top to second layer distance are only slightly smaller than those at $E = +1.00 \text{ V}$ (Table 1). The Hg overlayer is fitted with a density of $\rho_{\text{ads}} = 0.332 \pm 0.014$ and an atomic rms displacement $\sigma_{\text{ads}} = 0.44 \pm 0.06 \text{ \AA}$. However, this density is much lower than the value of 0.56 calculated from the hexagonal in-plane structure (with lattice constants $a = b = 3.86 \pm 0.03 \text{ \AA}$). This suggests that the Hg UPD overlayer forms two-dimensional islands on the Au(111) surface. At this potential, the bare Au surface is likely covered with a layer of water and some sulfate/bisulfate anions. The fitted Hg overlayer to Au(111) surface layer distance is $2.558 \pm 0.022 \text{ \AA}$ which is larger than the interlayer distance in bulk Au(111). Assuming that Hg and Au atoms are hard balls with diameters of 3.01 and 2.885 \AA , respectively, the Hg to Au(111) distance can be calculated as 2.570 \AA at bridge sites, 2.432 \AA at three-fold hollow sites, and 2.9475 \AA on atop sites. The fitted value is close to that at bridge sites and in between the other two extreme values, which is consistent with the averaged value over the incommensurate structure shown in Figure 3.

At $E = +0.63 \text{ V}$, the in-plane surface diffraction measurement shows the formation of Hg UPD phase II. However, the CTR profile (Figure 7c) has very similar features to that corresponding

TABLE 1: Specular CTR Fitting Parameters at Different Potentials

E (V)	adsorbate species	ρ_0	σ_0 (Å)	d_0 (Å)	ρ_{ads}	σ_{ads} (Å)	d_{ads} (Å)
+1.00 V	SO_4^{2-}	1	0.184 ± 0.012	2.406 ± 0.004	0.371 ± 0.02	0.2	2.082 ± 0.038
+0.68 V	Hg	1	0.165 ± 0.007	2.338 ± 0.0066	0.332 ± 0.014	0.44 ± 0.06	2.558 ± 0.022
+0.63 V	Hg	1	0.178 ± 0.0079	2.349 ± 0.0068	0.38 ± 0.11	0.75 ± 0.26	2.46 ± 0.14

to Hg UPD phase I (Figure 7b). This set of data can also be fitted with a single Hg overlayer on the relaxed Au(111) surface. The fitted parameters are $\rho_0 = 1$, $\sigma_0 = 0.178 \pm 0.0079$ Å, and $d_0 = 2.349 \pm 0.0068$ Å for the top Au(111) layer, and $\rho_{\text{ads}} = 0.38 \pm 0.11$, $\sigma_{\text{ads}} = 0.75 \pm 0.26$ Å, and $d_{\text{ads}} = 2.46 \pm 0.14$ Å for the Hg UPD layer. The density of the Hg layer is slightly higher than that corresponding to Hg UPD phase I, but much lower than 0.751 as calculated from the in-plane structure. Therefore, this Hg UPD overlayer also appears to be present as two-dimensional islands on the Au(111) surface. The distance from the Hg overlayer to the Au(111) surface is 2.46 ± 0.14 Å, which is smaller than the average values of 2.604 and 2.657 Å calculated from the two $c(2 \times 2)$ commensurate models shown in Figure 4, a and b, respectively. This might be due to a strong chemical bond between Hg and Au atoms. A similar phenomenon has been previously observed in TI UPD on Au(111).²² On the other hand, the rms displacement of Hg atoms of Hg UPD phase II (0.75 ± 0.26 Å) is much larger than that of Hg UPD phase I (0.44 ± 0.06 Å). Of the two models shown in Figure 4, model a would give an rms displacement much larger than that of model b, suggesting that model a is likely the correct one.

4. Discussion: The Kinetics of Hg UPD Phases

In the previous sections, we have presented the structures of two ordered Hg UPD phases at potentials of +0.68 and +0.63 V, respectively. Both of these phases are within the potential region of the broad reduction wave in Figure 1. The specular CTR data suggested that both phases are present as two-dimensional islands. We found that these two phases exhibited strong kinetic effects which might account for the broad reduction wave in the cyclic voltammetric response.

Hg UPD phase I was observed only when Hg was deposited on a freshly flame-annealed Au(111) electrode and was stable for about 3–4 h after being deposited. During CTR measurements of this phase, the Hg layer had to be stripped at +1.00 V and redeposited at +0.68 V every two hours to ensure that we were studying the same structure. However, after about 7–8 h past the initial deposition, phase I disappeared and we were not able to recover it without reannealing the crystal. Instead, the redeposited Hg UPD overlayer showed the structure of Hg UPD phase II. This phase was more stable and could be repeatedly stripped at $E > +0.90$ V and redeposited at $+0.50 \text{ V} \leq E \leq +0.70 \text{ V}$ as long as the deposition was within the monolayer regime. Hg UPD phase I could also be converted to Hg UPD phase II by changing the potential from +0.68 V (where Hg UPD phase I was observed) to +0.63 V. Clearly, Hg UPD phase I is a metastable structure whose instability is likely due, at least in part, to its partially charged chemical state.

Hg UPD phase II also shows some kinetic effects. This was found during specular CTR measurements. Typically, a set of specular CTR measurements consists of rocking curves at a series of Q_z 's, which takes more than 8 h to complete. The same rocking curve around (0, 0, 0.5) repeated after 6 h was found to have an intensity that was several times higher than before, suggesting that the structure of the Hg UPD changed during that time period. The intensity becomes constant again after the Hg UPD phase II is deposited for more than 12 h, so we believe that it forms yet another structure.

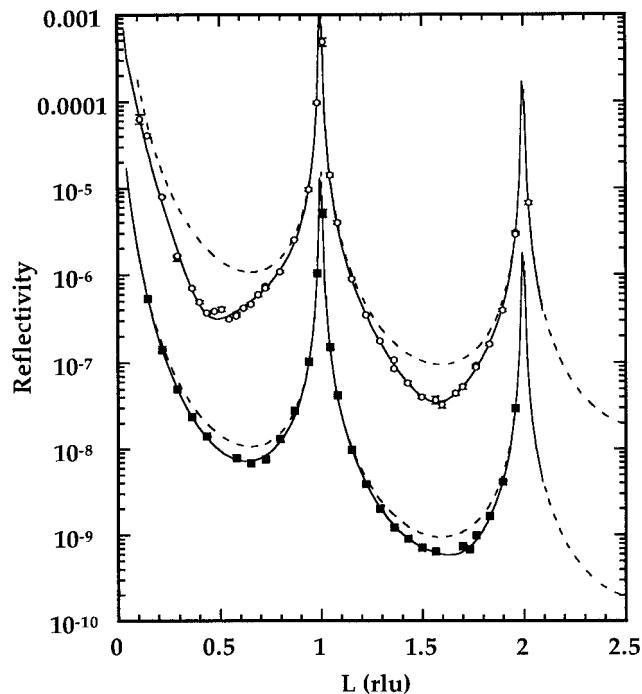


Figure 8. CTR corresponding to Hg UPD phase II (open circles) on the Au(111) electrode and that measured after holding potential at +0.63 V for 12 h (solid squares). The latter is shifted down by 2 orders of magnitude for a better view. Dashed lines are the calculated CTR curves for an ideal Au(111) electrode and continuous lines are fits to the data.

Figure 8 shows the specular CTR data of a freshly deposited Hg UPD phase II (open circles) along with that of the same sample measured after the Hg overlayer had been deposited and held at +0.63 V for more than 12 h (filled squares; displaced by 2 orders of magnitude to give a clearer view). The data for the fresh Hg UPD phase II was taken by stripping the Hg layer at +1.00 V and redepositing it at +0.63 V every 2 h. The other set of data was taken after 12 h without any other disturbance once the Hg had been deposited. In this case, there is a dramatic change in intensity around the anti-Bragg points and the CTR profile is close to that of an ideal Au(111) surface (dashed line).

As mentioned before, the CTR data of Hg UPD phase II could be fitted with a single layer of Hg on the Au(111) surface. On the other hand, the CTR data after 12 h could be fitted, with the same quality, by either a single Hg overlayer or a single water layer on the relaxed Au(111) surface. The fitted parameters are listed in Table 2. When fitted with a Hg overlayer, the parameters for the Au(111) surface are $\rho_0 = 1$, $\sigma_0 = 0.1004 \pm 0.0069$ Å, and $d_0 = 2.354 \pm 0.002$ Å. Fitting parameters for the Hg overlayer are $\rho_{\text{ads}} = 0.8916 \pm 0.0089$, $\sigma_{\text{ads}} = 0.0906 \pm 0.0093$ Å, and $d_{\text{ads}} = 2.344 \pm 0.004$ Å. The fitted coverage is consistent with a fully covered close-packed Hg layer (with a calculated coverage of 0.92). Both the rms displacement and the overlayer to substrate distance are close to the values of bulk Au(111) (0.085 and 2.3556 Å, respectively).

If fitted with a monolayer of water, the parameters for the Au(111) surface layer are about the same as before, with $\rho_0 = 1$, $\sigma_0 = 0.121 \pm 0.013$ Å, and $d_0 = 2.354 \pm 0.006$ Å. The parameters for the water overlayer are fitted as $\rho_{\text{ads}} = 0.768 \pm$

TABLE 2: Specular CTR Fitting Parameters for a Sample Held at $E = +0.63$ V for More Than 12 h

adsorbate species	ρ_0	σ_0 (Å)	d_0 (Å)	ρ_{ads}	σ_{ads} (Å)	d_{ads} (Å)
Hg	1	0.1004 ± 0.0069	2.354 ± 0.002	0.892 ± 0.0089	0.091 ± 0.0093	2.3442 ± 0.0041
H ₂ O	1	0.121 ± 0.013	2.354 ± 0.006	0.768 ± 0.082	0.2	2.12 ± 0.16

0.082, $\sigma_{\text{ads}} = 0.2$ Å, and $d_{\text{ads}} = 2.12 \pm 0.16$ Å. The rms displacement σ_{ads} was fixed at 0.20 Å to prevent it from going to zero. As mentioned before, the value of this parameter has little, if any, effect on the other fitting parameters. The fitted coverage of the water overlayer is a bit smaller than that for a Au(111) electrode in 0.10 M H₂SO₄ at +0.70 V. This is consistent with our previous result that the adsorbed water molecules are desorbed from the Au(111) surface when the potential is moved from +0.70 to +0.40 V.⁷

Thus, the specular CTR results suggest two possible models. In the first model, Hg deposition on the Au(111) surface continues when the potential is held at +0.63 V and a full monolayer of close-packed Hg is formed after about 12 h. This is based on the assumption that the Hg atoms are stable on the Au(111) surface without diffusing into the bulk if the deposition is within one monolayer. However, Hg is known to have a relatively high diffusion coefficient in bulk Au crystals. If Hg atoms on the Au surface were to diffuse into the bulk crystal, the Hg coverage would decrease with time rather than increase. After about 12 h, all the deposited Hg atoms would disappear from the surface assuming there is no more deposition from bulk solution. The disturbance to the bulk Au crystal might not be particularly dramatic since the total amount of Hg deposited would be less than one monolayer. Since the diameter of Hg atoms is 0.125 Å larger than that of Au atoms, this will induce only a small disturbance to the Au crystal. Thus, the second model of a weakly adsorbed water layer on the Au(111) surface cannot be rigorously excluded.

Based on the specular CTR data alone, it is difficult to unambiguously determine which is the correct model. However, previous electrochemical studies have found that the Hg overlayer might form an intermetallic compound with the Au substrate.^{8–12} Since alloy formation would likely change the electrochemical properties of the Au electrode, one could, based on the electrochemical response prior to and after the formation of this structure, distinguish between these two models. Figure 9 shows the cyclic voltammograms of a Au(111) electrode in 0.10 M H₂SO₄ solution containing 0.10 mM Hg²⁺ at a scan rate of 20 mV/s. Curve A (thin line) was measured with a fresh flame-annealed Au(111) crystal and curve B (thick line) was measured after depositing Hg at +0.63 V for about 12 h. The fresh Au(111) sample shows a pair of sharp peaks around +0.90 V similar to the features shown in Figure 1. The cathodic wave was broadened due to the relatively low Hg²⁺ concentration (0.10 mM). After holding the potential at +0.63 V for 12 h, the pair of sharp peaks around +0.90 V is replaced by a pair of broad peaks around +0.76 V. The peak position is shifted negatively by 140 mV, and the separation in peak potentials increased relative to a fresh Au(111) crystal. Clearly, after 12 h, the Hg-surface interaction is weaker and more negative potentials are required for the Hg deposition. This change could be due to the formation of a layer of an intermetallic compound or a full Hg monolayer. On the other hand, it cannot be readily explained by the second model which should give rise to a clean Au(111) surface.

Careful examination of Figure 9 also shows that a very small wave at about +0.76 V is also present in the CV taken with a fresh Au(111) electrode (curve A). This wave (to which we alluded to earlier, section 3.1) is also present in the inset of Figure 1. It is consistent with the assumption that it corresponds

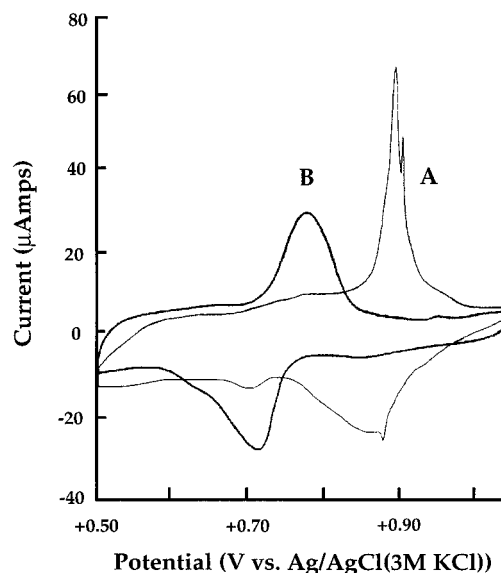


Figure 9. Cyclic voltammograms of a Au(111) electrode in 0.10 M sulfuric acid containing 0.10 mM Hg²⁺ at a scan rate of 20 mV/s. Curve A (thin line) was measured with a fresh flame-annealed Au(111) crystal and curve B (thick line) was measured after depositing Hg at +0.63 V for about 12 h.

to the fully discharged metallic mercury on the Au(111) surface. The amount of mercury in this state is very small on a fresh Au(111) surface but builds up slowly. We found that this process is strongly dependent on the potential at which the electrode is held, the Hg²⁺ concentration, and the types of anions present in solution. Detailed electrochemical studies are underway and will be published elsewhere.²⁰

To further understand this kinetic process, we carried out both rocking scans across (0, 0, 0.5) and in-plane radial scans following the deposition of Hg over a 12 h period. Figure 10a shows the integrated intensity under the rocking curve vs time which reflects the change in the surface normal structure during the kinetic process. Clearly, there is a dramatic change after about 6 h. Between 0 to 5 h and 7 to 12 h, there appear two plateaus. The two sets of data shown in Figure 8 were taken in these two regions, respectively. The peak width of the in-plane radial scan first decreased slightly and then increased after 6–8 h (see Figure 10b). This indicates that the domain size of the Hg UPD layer first increases and then decreases. However, the change is small (about 20%). On the other hand, the integrated intensity of the in-plane radial scan first increases and then decreases after about 6 h (see Figure 10c). Since this quantity is proportional to the total amount of Hg atoms in the ordered surface layer, one can conclude that the ordered Hg UPD islands likely grow at first. After about 6 h, some of them appear to change to a third phase which gives no in-plane surface diffraction. This phase could be either a liquid Hg overlayer or a layer of an amorphous Hg–Au intermetallic compound or alloy. However, at this time, we do not have any direct experimental evidence to derive the details of this structure.

We can speculate that the formation of the third phase requires a certain critical size or coverage of the Hg overlayer. Once the islands grow over this size (after about 6 h), they may coalesce to form a 2-D liquid or an amorphous structure. This was indicated by the specular CTR data in Figure 10a. The intensity at (0, 0, 0.5) shows a transition at about 6 h consistent

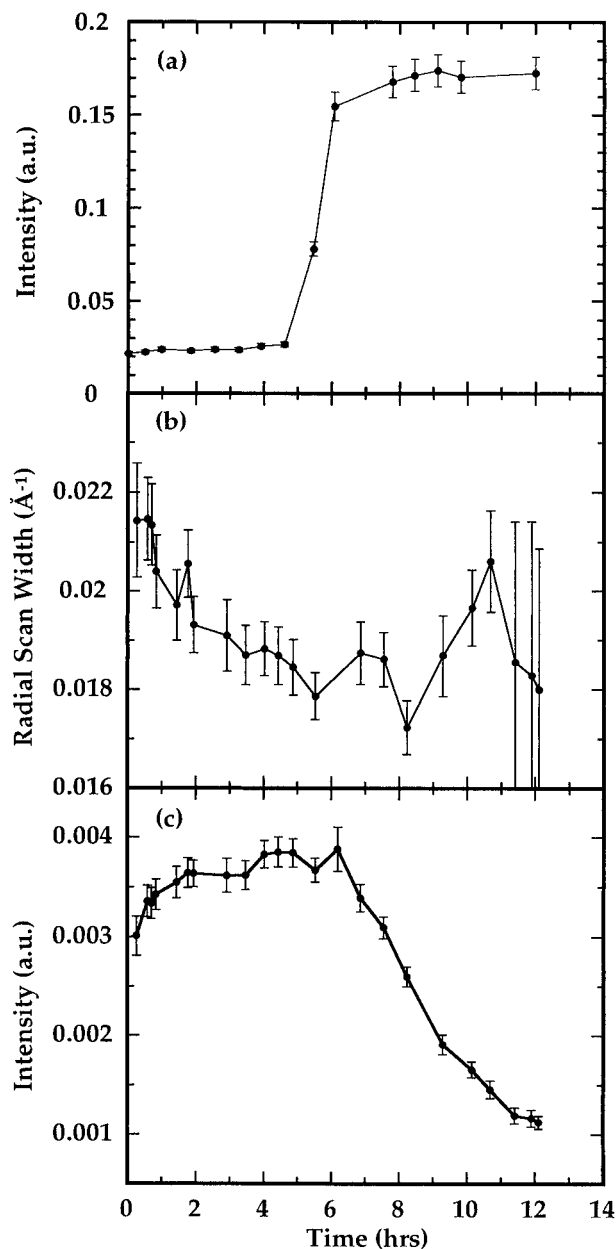


Figure 10. X-ray scattering intensity changes during Hg UPD at +0.63 V: (a) integrated intensity of the rocking curve across specular CTR at (0,0,0.5); (b) full width at half-maximum of the in-plane radial scan across (1,0)_{II} of Hg UPD phase II; (c) integrated intensity of the in-plane radial scan across (1,0)_{II}.

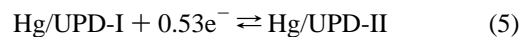
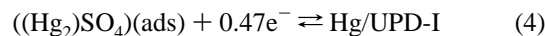
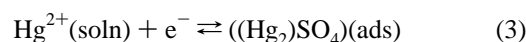
with the in-plane data. A 2-D island growth model would predict a continuous increase in the overlayer density before the sudden jump at about 6 h to form a 2-D liquid or an amorphous structure. However, a detailed understanding would require a series of time-resolved specular CTR data. Unfortunately, it is not feasible in this case since it takes about 8 h to complete the measurement of one set of specular CTR data. Future experiments using time-resolved X-ray scattering techniques would be most valuable in exploring the transition processes³⁰ and we are currently exploring such possibilities.

At this stage, it is not well understood why the kinetics of reducing mercury ions to the fully discharged metallic state is so slow. It could be due to anion-coadsorption effects, a disproportionation reaction involving the adsorbed intermediate(s), or slow nucleation processes. We have carried out both GIXD and specular CTR measurements in solutions containing different anions such as SO_4^{2-} , ClO_4^- , Cl^- , and CH_3COO^- and the results clearly show a strong anion dependence of the

structures involved in Hg UPD. Further studies are in progress to elucidate the effects of anions on the kinetics of Hg UPD on Au surfaces.³¹

Our results can be compared with previous electrochemical kinetic studies of Hg UPD on polycrystalline Au electrodes. As mentioned before, Salié and Bartels^{13–16} proposed that initially Hg(II) is rapidly reduced to Hg(I) and then slowly reduced to a fully discharged metallic layer through two intermediate states. In our previous paper,⁷ we reported on the formation of a Hg_2SO_4 layer (with mercury present as mercurous dimers) at the initial stages of Hg UPD. Starting from this potential ($+0.80 \text{ V} \leq E \leq +0.88 \text{ V}$) and scanning to more negative values, we observed two ordered Hg UPD structures which are in excellent qualitative agreement with the mechanism proposed by Salié and Bartels. They describe the underpotential deposition of a metal according to a general theory of chemisorption reactions with multiple steps.^{13–16}

In the present case, the deposition process can be described by eqs 3–6.



where $\text{Hg}^{2+}(\text{soln})$, $((\text{Hg}_2)\text{SO}_4)(\text{ads})$, Hg/UPD-I, Hg/UPD-II, and Hg^0/UPD represent, respectively, mercuric ions in solution, adsorbed mercurous sulfate, UPD phases I and II, and the metallic mercury overlayer. Potentiostatic measurements with a polycrystalline Au ring-disk electrode and impedance spectroscopy on a polycrystalline Au electrode have been employed to determine the partial charge on the electrodeposited mercury species.^{13–16} Assuming similar values for single-crystal Au(111) electrodes, we expect that the charge of each Hg atom is about $0.53e^-$ in Hg UPD phase I and close to zero in Hg UPD phase II. These values are consistent with the open structure of Hg UPD phase I as being due to the Coulombic repulsion forces between the partially charged Hg atoms. In Hg UPD phase II, the commensurate structure may be at a local free energy minimum and thus would be more stable than phase I. Finally, the transition from Hg UPD phase II to the fully discharged 2-D liquid Hg or amorphous alloy structure is also consistent with the last alloy formation step according to the studies by Salié and Bartels.

5. Conclusions

In summary, we report on two ordered intermediate Hg UPD phases and a fully discharged 2-D liquid Hg or an amorphous Hg–Au alloy structure during the UPD of Hg on Au(111) electrodes in 0.10 M H_2SO_4 solution. These results, combined with our previous report on the first stage of Hg UPD on Au(111) electrodes, present a detailed understanding of the UPD of Hg from Hg(II) to a fully discharged metallic state. Both ordered intermediate phases have hexagonal structures with lattice vectors rotated 30° relative to those of the Au(111) substrate. The first phase was observed only on a fresh flame-annealed Au(111) electrode at an applied potential of +0.68 V. It is incommensurate with the Au(111) surface with lattice constants $a = b = 3.84 \pm 0.03 \text{ \AA}$. The open, incommensurate, structure is likely due to the Coulombic repulsion forces between the partially charged Hg atoms. We found that this phase is a metastable state which changes with time (on a time scale of

3–4 h), as well as with potential (at $E \leq +0.63$ V), to a second phase. This is a more compact phase with lattice constants $a = b = 3.328 \pm 0.01$ Å which are about 10.6% larger than the close packing distance in bulk Hg. It is likely a commensurate $c(2 \times 2)$ structure with $2/3$ of the Hg atoms at threefold hollow sites and $1/3$ at on-top sites. By holding the potential at $E = +0.63$ V for extended time periods, more Hg atoms appear to be deposited onto the Au(111) surface and form larger two-dimensional islands. After about 12 h, the underpotentially deposited Hg monolayer is transformed to either a monolayer of fully discharged liquid Hg or a monolayer of an amorphous Hg–Au intermetallic compound. The entire Hg UPD process, from Hg(II) to the fully discharged Hg on the Au(111) surface in sulfuric acid, agrees well with the mechanism proposed by Salié and Bartels based on their electrochemical kinetic studies. The UPD of Hg on Au(111) electrodes shows a unique mechanism quite different from UPD processes of other metals such as Cu, Ag, Tl, and Pb.

Acknowledgment. This work was supported by the Office of Naval Research and the National Science Foundation (CHE9407009). Most synchrotron X-ray experiments were performed at Exxon beamline $\times 10B$ at the National Synchrotron Light Source, Brookhaven National Laboratory, which is supported by the U.S. Department of Energy, Division of Materials Science and Division of Chemical Sciences (DOE contract No. DE-AC02-76CH0016). Preliminary X-ray measurements were also performed at the Cornell High Energy Synchrotron Source, which is supported by National Science Foundation. We thank Dr. K. Liang for his technical help and scientific discussions. We also thank Sean Smith, Shaowei Chen, and Dr. Enrique Herrero for participating in parts of these experiments and for their helpful suggestions and discussions.

References and Notes

- Magnussen, O. M.; Hotlos, J.; Nichols, R. J.; Kolb, D. M.; Behm, R. J. *Phys. Rev. Lett.* **1990**, *64*, 2929.
- Hachiya, T.; Honbo, H.; Itaya, K. *J. Electroanal. Chem.* **1991**, *315*, 275.
- Manne, S.; Hansma, P. K.; Massie, J.; Elings, V. B.; Gewirth, A. A. *Science* **1991**, *251*, 183.
- Abruña, H. D. In *Advances in Chemical Physics*; Prigogine, I., Rice, S. A., Eds.; John Wiley & Sons, Inc: New York, 1990; Vol. LXXVII, p 255.
- Toney, M.; McBreen, J. *Electrochem. Soc.* **1993**, *2* (1), 22.
- Toney, M. F.; Ocko, B. M. *Synchrotron Radiat. News* **1993**, *6* (5), 28.
- Li, J.; Abruña, H. D. *J. Phys. Chem.* **1997**, *101*, 244.
- Lindstrom, T. R.; Johnson, D. C. *Anal. Chem.* **1981**, *53*, 1855.
- Schadewald, L. A. *J. Electrochem. Soc.* **1984**, *131*, 1583.
- Sherwood, W. G.; Bruckenstein, S. *J. Electrochem. Soc.* **1978**, *125*, 1098.
- Sherwood, W. G.; Untereker, D. F.; Bruckenstein, S. *J. Electrochem. Soc.* **1978**, *125*, 384.
- Shay, M.; Bruckenstein, S. *Langmuir* **1989**, *5*, 280.
- Salié, G.; Bartels, K. *J. Electroanal. Chem.* **1988**, *245*, 21.
- Batels, K.; Salié, G. *Z. Phys. Chem.* **1990**, *271*, 739.
- Salié, G.; Bartels, K. *Electrochim. Acta* **1994**, *39*, 1057.
- Salié, G. *J. Electroanal. Chem.* **1989**, *259*, 315.
- Vicente-Beckett, V. A. *Aust. J. Chem.* **1989**, *42*, 2107.
- Chen, C.-H.; Gewirth, A. A. *Phys. Rev. Lett.* **1992**, *68* (10), 1571.
- Inukai, J.; Sugita, S.; Itaya, K. *J. Electroanal. Chem.* **1996**, *403*, 159.
- Herrero, E.; Li, J.; Abruña, H. D., manuscript in preparation.
- Toney, M. F.; Gordon, J. G.; Samant, M. G.; Borges, G. L.; Melroy, O. R. *J. Phys. Chem.* **1995**, *99*, 4733.
- Wang, J. X.; Adzic, R. R.; Ocko, B. M. *J. Phys. Chem.* **1994**, *98*, 7182–7190.
- Toney, M. F.; Howard, J. N.; Richer, J.; Borges, G. L.; Gordon, J. G.; Melroy, O. R.; Yee, D.; Sorensen, L. B. *Phys. Rev. Lett.* **1995**, *75* (42), 4472.
- Chen, C.-h.; Kepler, K. D.; Gewirth, A. A.; Ocko, B. M.; Wang, J. *J. Phys. Chem.* **1993**, *97*, 7290–7294.
- Wang, J. X.; Adzic, R. R.; Magnussen, O. M.; Ocko, B. M. *Surf. Sci.* **1995**, *335*, 120–128.
- Wang, J. X.; Adzic, R. R.; Magnussen, O. M.; Ocko, B. M. *Surf. Sci.* **1995**, *344*, 111–121.
- Wang, J.; Ocko, B. M.; Davenport, A. J.; Isaacs, H. S. *Phys. Rev. B* **1992**, *46* (16), 10321.
- Gibbs, D.; Ocko, B. M.; Zehner, D. M.; Mochrie, S. G. *J. Phys. Rev. B* **1988**, *38*, 7303.
- International Tables for X-ray Crystallography*; Ibers, J. A., Hamilton, W. C., Eds.; Kynoch: Birmingham, U.K., 1974; Vol. IV.
- Finnefrock, A. C.; Buller, L. J.; Ringland, K. L.; Brock, J. D.; Abruña, H. D. *J. Am. Chem. Soc.*, submitted for publication.
- Li, J.; Herrero, E.; Abruña, H. D., manuscript in preparation.